



Received August 04, 2025; accepted October 21, 2025; Date of publication October 29, 2025. The review of this paper was arranged by Associate Editor Fernanda de M. Carnielutti® and Editor-in-Chief Heverton A. Pereira®. Digital Object Identifier http://doi.org/10.18618/REP.e202555

Decentralized Control Strategy for a Stand-Alone DC Microgrid based on **Voltage Droop and Virtual Impedance**

Maico S. Lima^{⊚1}, Renan R. Almeida^{⊚1}, Andrei O. Almeida^{⊚1,∗}

¹Centro Federal de Educação Tecnológica de Minas Gerais, Programa de Pós-Graduação em Automação e Sistemas, Leopoldina, MG,

e-mail: maicolima.leopoldina@cefetmg.br; renanrocha529@gmail.com; and rei.almeida@cefetmg.br * the control of the control ofCorresponding author.

ABSTRACT The continuous development of photovoltaic and energy storage systems has enabled the emergence of microgrids, which can operate with alternating or direct current (DC), depending on the components characteristics. Since photovoltaic panels and battery storage systems operate in DC, connecting them via a DC bus simplifies power conversion, especially for DC loads. A key challenge in microgrids is defining an effective control strategy, which may be centralized, decentralized, or distributed. In this sense, the main proposal of this paper consists in the development of a decentralized control strategy for a stand-alone DC microgrid with photovoltaic generation and battery energy storage, using a controlled voltage droop, based on virtual impedance. This paper aims to contribute with the description of the implementation steps of the local controllers, using classical control techniques based on transfer function modelling. In addition, the assembling steps of a low-cost and small-scale DC microgrid prototype are presented. The control approach maintains DC bus voltage within an appropriate range without requiring communication among system components. Moreover, it supports modular expansion by enabling the seamless integration of new generation or storage units. To validate the strategy, a microgrid prototype was developed using a 60 W PV panel, a 12 V, 7 Ah lead-acid battery, and the BOOSTXL-3PhGaNInv evaluation module with a F28379D digital signal controller for converter implementation. Experimental results, including the battery charging process and variations of solar irradiance and load demand, demonstrate the effectiveness and robustness of the proposed control system.

KEYWORDS Battery Energy Storage Systems, DC Microgrids, Photovoltaic Systems, Virtual Impedance, Voltage Droop.

I. INTRODUCTION

In recent decades, the pursuit of energy transition has led to changes in the electrical system, such as the development of renewable energy sources and the concept of distributed generation. Within this new scenario, the concept of microgrids has emerged [1]. Microgrids can be understood as electrical networks that include elements such as self-generation and energy storage systems, and can be stand-alone or connected to the main grid, in order to serve local loads.

In the past decades, the growing search for renewable energy sources has driven the development of stand-alone photovoltaic (PV) systems, which emerges as a viable alternative for meeting energy demand in remote areas, not served by the main grid [2]. Compared to other energy sources, such as wind and biodiesel generators, photovoltaic energy has some advantages, such as greater flexibility for small or large-scale generation, silent operation, and no need for fuel transportation [3].

Another central role in microgrids is played by battery energy storage systems (BESS), which allow for the management of energy production and consumption, taking into account load variations and intermittent generation. Recently,

energy storage has become more attractive, even for largescale power systems, due to recent advances in lithium-ion batteries [4] and green hydrogen technologies [5].

Regardless of whether the microgrid is connected to the main grid or not, its structure can be designed using alternate (AC) or direct current (DC). If the microgrid consists of DC sources, such as photovoltaic panels and batteries, using a DC structure, where the elements are connected by a DC bus, can simplify the conversion stages. Even for AC generation sources such as wind turbines, the conversion steps can be simplified, as only one rectifier stage would be needed. In this sense, greater system efficiency and lower implementation costs are expected [6].

The development of DC microgrids has several challenges, related to technical, economical and regulatory aspects. As the main technical challenges of DC microgrids, is possible to cite [7]:

• Voltage fluctuations: different of the AC microgrids, where the frequency and voltage regulation can be independently achieved by the active and reactive power control, in DC microgrids are more sensitive to voltage



fluctuations, especially when different energy sources are used. To overcome this issue, different control strategies were proposed in the literature [8];

- Energy management: the DC microgrids are often proposed to integrate intermittent renewable energy sources, which demands an energy storage system (ESS) to balance the energy consume and storage in different conditions of load and generation, as well as a control strategy to achieve this in an efficient manner [9];
- Energy storage balancing: the charging and discharging of distributed ESS bring to a challenge on balancing method for their state-of-charge (SoC). For this issue, two main control approaches are proposed, being the master-slave and the distributed control [10];
- Fault detection and clearing mechanisms: DC microgrid may face fault currents with high magnitude and fast variation, due to the high discharge of capacitive filters and low-impedance DC cables. In addition, the non-zero crossing makes it necessary more complex protection mechanisms to interrupt the fault currents. Furthermore, the bidirectional power flow characterized by the ESS difficult the fault detection [11].
- DC arc detection and interruption: a DC arc can be caused by insulation damage, a loosing joint connection or external influence. As the fault currents, a DC arc does not have zero-crossing point when compared to an AC arc. In addition, the DC arc introduces a resistance, reducing the current, which can mislead the conventional protection devices [12]. Besides that, a DC arc can cause undesirable control actions, especially if a communication system is used between the converter units [13].

Most of the above cited issues may be mitigated with an adequate control strategy. In literature, three general approaches are discussed: centralized, decentralized or distributed [14].

Figure 1(a) illustrates the centralized control strategy, also known as master-slave strategy. In this strategy, a master converter controls the DC bus voltage and determines how much power the other converters must inject into the DC bus, or for batteries, how much power must be consumed or injected [15]. As an advantage, with a centralized control, is possible to achieve an optimum operation condition, optimizing the use of resources. However, failures in communication between the master converter and the others may compromise the entire operation.

Figure 1(b) shows a schematic diagram of the decentralized control approach, using a voltage droop. In this strategy, each converter operates without communication between them, leaving the DC bus voltage unregulated [16]. A widely used approach is the implementation of virtual impedance at the DC bus connection point. In this method, an increase in the current supplied by the converter leads to a reduction, or a droop, in the output voltage. For each converter, the droop controller determines the power reference to be injected into the system based on the measured DC bus voltage.

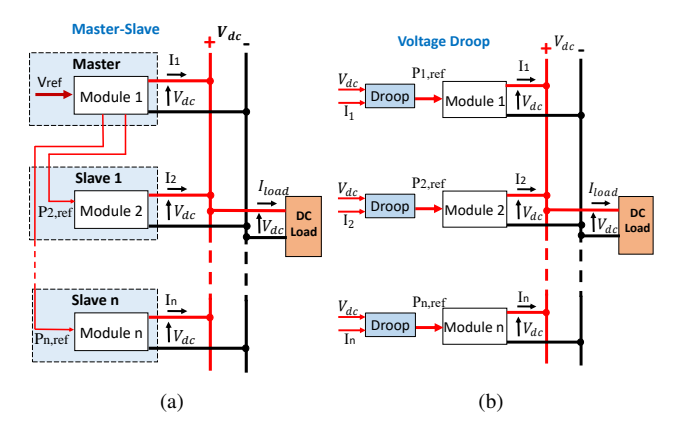


FIGURE 1. Schematic diagram of DC microgrids control strategies: (a) centralized or master-slave and (b) decentralized or voltage droop.

Distributed control is very similar to the centralized strategy, but the microgrid is divided into subsystems, being each with it own master converter. This approach allows the optimal operation in each subsystem, however it does not eliminate the communication between different parts of the

The selection of an appropriate control strategy depends on the specific characteristics and operational requirements of the microgrid. If the sources are close to each other, the centralized control may optimize the system operation. However, the system expansion is harder with a centralized control, because the management of the energy sources changes with the expansion. On the other hand, the decentralized control is not affected by the distance between converters and allows an easy expansion of the system, as long as the system components are designed for this.

Mostly decentralized strategies use a droop control technique, which can be implemented using different approaches [17]. For example, in [9] a classical power-to-voltage droop is implemented in a grid-connected DC nanogrid, using the concept of net zero energy. The microgrid is modelled in a hardware-in-the-loop (HIL) real time simulator, using detailed models of a PV panel, batteries and a electrical vehicle charger.

In [18] is proposed a droop control strategy for DC micrgrids using the concept of virtual impedance. In this proposal, the droop is adaptative and aims to balance the DC voltage stability and the current sharing, which is done with a communication system between the converters. The proposal is tested experimentally using two controlled DC sources in parallel.

Similar to the approach of [18], in [19] is proposed a robust droop control strategy for DC micrgrids using the concept of virtual impedance. In this proposal, the droop is adaptative and aims to balance the DC voltage stability and the current sharing, which is done with a communication system between the converters. The proposal is tested experi-



mentally using controlled AC sources and AC/DC converters with Neutral Point Clamped (NPC) topology. Also, a similar approach is proposed in [20], but using fuzzy logic to improve the DC voltage stability and the current sharing.

In [21] a theoretical study is presented, proving that the virtual resistance is a loss-free resistor and verify this with digital simulations. Even though this reference does not propose a new strategy, this study helps to understand the virtual resistance behaviour and how to implement a droop control based on virtual resistance.

In [22], a decentralized control strategy was proposed for a series-connected wind farm, using a controlled current droop based on virtual admittance. Inspired in this concept, the main proposal of this paper consists in the development of a decentralized control strategy for a stand-alone DC microgrid with photovoltaic generation and BESS, using a controlled voltage droop, based on virtual impedance. This paper aims to contribute with the description of the implementation steps of the local controllers, using classical control techniques based on transfer function modelling. In addition, the assembling steps of a low-cost and small-scale DC microgrid prototype are presented.

Figure 2 shows the block diagram of the voltage controller $C_d(s)$ with a virtual impedance feed-back R_v . This controller is used in all sources of the microgrid, as shown in 1(b), and generates a reference value for the current to be injected at the DC bus. If all converters try to control the DC bus voltage V_{dc} , it leads to a conflict between the controller. Therefore, the virtual impedance allows to change the voltage reference according to the current supplied, implement a droop characteristic:

$$V_{dc}^{'*} = V_{dc}^* - R_v I_n \tag{1}$$

 $V_{dc}^{'*}=V_{dc}^*-R_vI_n \eqno(1)$ where $V_{dc}^{'*}$ is the corrected reference value, V_{dc}^* is the open circuit voltage and I_n is the current to be injected into the DC bus by the n^{th} module. Note that, this approach does not implements a linear droop curve as in the classic droop strategies, where a power reference value is defined according to the DC bus voltage. The value of R_v can be chose according to the power source bounds, as will be discussed later in this work.

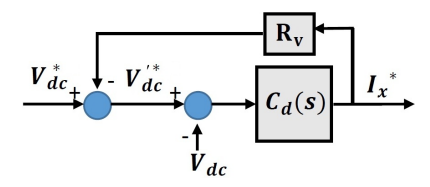


FIGURE 2. Block diagram of the voltage droop controller based on virtual impedance.

In order to test the proposed control strategy, a small-scale microgrid prototype was implemented using a 60 W photovoltaic panel, a 12 V/7 Ah lead-acid battery, resistive DC loads and converters built from a BOOSTXL-3PhGaNInv three-phase module controlled by a LAUNCHXL-F28379D digital signal processor (DSP) [23].

Having in mind the above presented introduction, especially the brief description of other droop control methods applied to DC microgrids, the main contributions of this paper can be listed as follows:

- A detailed implementation of a droop control strategy based on virtual impedance;
- A design method for the controllers parameters in the frequency domain;
- An experimental validation using a real PV panel and a real lead-acid battery, instead of controlled sources.
- A description of the implemented small-scale and lowcost prototype of a DC microgrid with a PV panel and a lead-acid battery, which can be expanded using other sources and also be used to test other control strategies.

The remainder of this paper is organized as follows: Section II presents the mathematical modeling of the system components and the controller design. Section III details the prototype implementation, including the components used. Section IV discusses the experimental results from various tests conducted on the DC microgrid. Finally, Section V provides the concluding remarks.

II. MODELLING AND CONTROL OF THE DC MICROGRID **COMPONENTS**

Figure 3 shows a schematic diagram of the proposed DC microgrid, with a PV panel and a lead-acid battery connected to half-bridge converters in boost configuration, feeding two DC loads connected in parallel with the DC bus.

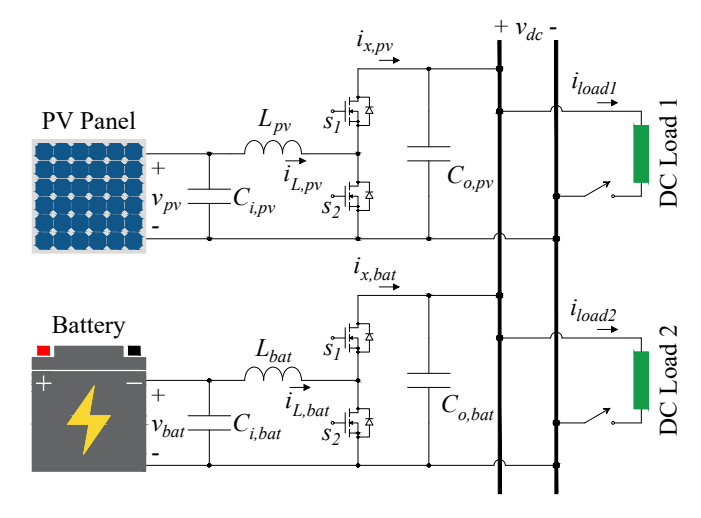


FIGURE 3. Schematic diagram of the proposed DC microgrid with the equivalent circuits of the half-bridge converters.

In each converter, the inductor current is controlled through an inner loop. The current reference of each converter is generated by the droop controller, which works as an outer loop. In addition, the voltage at the battery terminals is controlled during the final stage of the charging process. In the following sections, each part of the overall control strategy will be discussed.

A. Current Control

Having in mind the currents direction in Figure 3 and considering initially as constant the DC bus and the PV panel voltages, the dynamic behaviour of the inductor current can be described as:

$$L_{pv}\frac{di_{L,pv}}{dt} + R_{pv}i_{L,pv} = V_{pv} - V_x, \tag{2}$$

where L_{pv} and R_{pv} are the inductance and resistance of the inductor, respectively, $i_{L,pv}$ is the inductor current, V_{pv} is the PV panel terminal voltage and V_x is the voltage of the lower switch S_2 , given by:

$$V_x = DV_{dc} \tag{3}$$

where D is the duty cycle of the converter and V_{dc} is the DC bus voltage. Replacing (3) in (2) and applying the Laplace transform in the result equation, the closed loop block diagram of Figure 4 can be defined. The -1 gain before the controller $C_i(s)$ is used because the current direction was modelled from the PV panel to the converter.

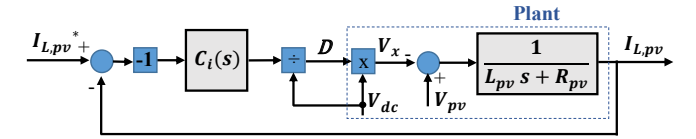


FIGURE 4. Block diagram of the inductor current control.

Considering the PV panel voltage V_{pv} as a disturbance in the control diagram and using a proportional-integral (PI) controller in $C_i(s)$, the open loop transfer function is written as:

$$\frac{I_L(s)}{E(s)} = \frac{k_{pi} \left(s + \frac{k_{ii}}{k_{pi}}\right)}{sL_{pv} \left(s + \frac{R_{pv}}{L_{pv}}\right)},\tag{4}$$

where k_{pi} and k_{ii} are the proportional and integral gains of the PI controller $C_i(s)$. Choosing the gains in such a way that the controller zero cancels the plant pole [24], the closed loop transfer function can be written as:

$$\frac{I_L(s)}{I_L^*(s)} = \frac{1}{1 + \left(\frac{L_{pv}}{k_{pi}}\right)s} = \frac{1}{1 + \tau s},\tag{5}$$

where τ is the time constant of the closed loop system, which can be chosen to design the gains as:

$$k_{pi} = \frac{L_{pv}}{\tau}$$
 and $k_{ii} = \frac{R_{pv}}{\tau}$. (6)

The current control loop of the battery converter can be implemented using the same technique presented, however, the inductance and resistance values of the battery converter, L_{bat} and R_{bat} , must be used. In addition, the time constant τ of the PV panel and battery control systems can be different, according to the ratings of each one.

B. Battery Voltage Control

In the literature, several methods have been proposed for the battery charging process. Some of the main charging methods can be cited: constant current, constant voltage, multi-step constant current, pulse charging and constant current constant voltage (CCCV) [25]. The CCCV method is a widely used method for lead-acid and lithium-ion batteries, since it preserves the battery lifespan and is easy to implement in a microcontroller. Therefore, the CCCV method is used in this work.

Figure 5 shows curves of voltage, current and SoC in an example of CCCV method application. The battery starts at its nominal voltage of 1 pu and is charged with constant current. When the voltage reaches its maximum value of 1.2 pu, the battery begins charging with constant voltage and the current is slowly reduced until the SoC reaches 1 pu. Therefore, to implement the CCCV method, it is necessary to control the battery voltage.

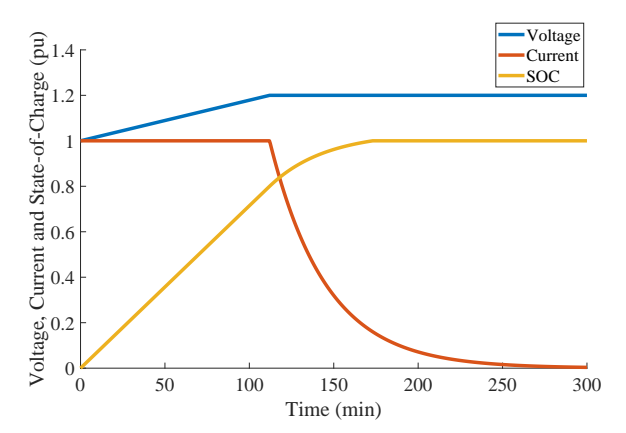


FIGURE 5. CC-CV charging method: curves of voltage, current and state of charge, all in pu.

Bearing in mind the circuit of Figure 3, the dynamic behaviour of the battery voltage can be described as:

$$C_{i,bat}\left(\frac{dv_{bat}}{dt}\right) = i_{bat} - i_{L,bat},\tag{7}$$

where $C_{i,bat}$ is the capacitance at the battery terminals, i_{bat} is the battery current and $i_{L,bat}$ is the inductor current. Applying the Laplace transform in (7), it is possible to draw the closed-loop block diagram of Figure 6. The voltage control is an outer loop, which generates a reference value for the inductor current. The gain -1 is used due to the direction adopted for the currents in the circuit.



FIGURE 6. Block diagram of the battery voltage control.

Considering the current I_{bat} as a disturbance and ensuring a faster response of the current inner loop, this is, with a time constant much smaller than the voltage outer loop, the following closed loop transfer function can be written:

$$\frac{V_{bat}(s)}{V_{bat}^{*}(s)} = \frac{\left(\frac{k_{pv,bat}}{C_{i,bat}}\right)s + \left(\frac{k_{iv,bat}}{C_{i,bat}}\right)}{s^2 + \left(\frac{k_{pv,bat}}{C_{i,bat}}\right)s + \left(\frac{k_{iv,bat}}{C_{i,bat}}\right)},$$
(8)

where $k_{pv,bat}$ and $k_{iv,bat}$ are the proportional and integral gains of the PI controller $C_v(s)$, respectively. Comparing the denominator of (8) with the canonical form $D(s) = s^2 +$ $2\xi\omega_n s + \omega_n^2$, where ω_n is the undamped natural frequency and ξ is the damping ratio, it is possible to design the controller

$$k_{pv,bat} = 2\xi \omega_n C_{i,bat}$$
 and $k_{iv,bat} = \omega_n^2 C_{i,bat}$. (9)

Since the canonical form does not have a zero in its numerator as (8), the step response can present a greater overshoot than expected for a chosen value of damping ratio. Furthermore, the presented mathematical modelling and controller design method can be used for a voltage controller applied to the PV panel converter.

C. Controlled Voltage Droop with Virtual Impedance

The droop controller is implemented as an outer loop to the current control and is used in the converters of both the PV panels and the batteries. However, unlike the voltage controller at the battery terminals, the droop controller does not use a fixed reference. If all converters attempted to control the DC bus voltage, they would conflict with each other, potentially causing system collapse. In this sense, the DC bus voltage reference is adjusted by a virtual impedance, according to the current supplied or consumed by each converter.

Once again, considering the current directions in Figure 3, the dynamics of the DC bus voltage can be described as:

$$\frac{dv_{dc}}{dt} = \frac{1}{C_{eq}}(i_{x,pv} - i_{load}),\tag{10}$$

where $C_{eq} = C_{o,pv} + C_{o,bat}$ is the DC bus equivalent capacitance, $i_{load} = i_{load1} + i_{load2}$ is the current demanded by he loads, $i_{x,pv}$ and $i_{x,bat}$ are the converters output currents of the PV panel and battery. By employing a pulsewidth modulation (PWM) strategy and assuming a switching frequency significantly higher than the variations in the duty cycle (d), the output current of the converters can be generally expressed as $i_x(t) = d(t)i_L(t)$, without specifying whether it refers to the battery or PV panel converter.

Applying the Laplace transform in (10), it is possible to draw the closed-loop block diagram of the droop controller with virtual impedance, as shown in Figure 7. Although a constant voltage reference is provided to the control system, it is not directly processed by the controller $C_d(s)$. Instead, the reference is adjusted by the virtual impedance R_v based on the output current i_x .

Initially neglecting the virtual impedance and considering the current control loop as unity gain, since this is much

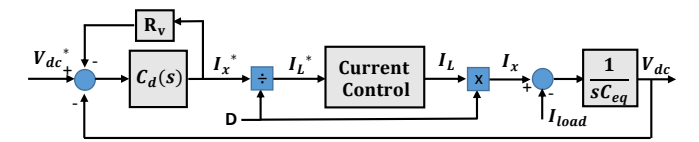


FIGURE 7. Block diagram of the controlled voltage droop strategy, with a

faster than the outer loop, the closed loop transfer function of the block diagram of Figure 7 can be written as:

$$\frac{V_{dc}(s)}{V_{dc}^{*}(s)} = \frac{\left(\frac{k_{pd}}{C_{eq}}\right)s + \left(\frac{k_{id}}{C_{eq}}\right)}{s^{2} + \left(\frac{k_{pd}}{C_{eq}}\right)s + \left(\frac{k_{id}}{C_{eq}}\right)},$$
(11)

where k_{pd} and k_{id} are the proportional and integral gains of the PI controller $C_d(s)$. These gains can be designed using the same method presented in subsection B, being calculated as:

$$k_{pd} = 2\xi\omega_n C_{eq}$$
 and $k_{id} = \omega_n^2 C_{eq}$. (12)

As discussed in the Introduction, one of the main challenges of the DC micorgrids is the choice between prioritizing current sharing or voltage regulation. The virtual impedance design is directly related to this choice. To prioritize the current sharing, an adaptive virtual impedance could be a better choice, since it can change according to the operation conditions. However, in this paper, the voltage regulation is prioritized, defining a minimum voltage at the DC bus for the worst-case scenario, in which the converter delivers its maximum current to the DC bus.

Therefore, prioritizing the voltage regulation and considering the worst scenario to ensure a minimum voltage level at maximum load conditions, the virtual impedance R_v can be designed as:

$$R_v = \frac{V_{dc}^* - V_{dc,min}}{I_{x,max}}. (13)$$

The voltage reference V_{dc}^{*} can be interpreted as the opencircuit voltage of a generator, which may vary during operation. For instance, it can be adjusted to maintain the rated DC bus voltage under maximum load conditions, or alternatively, under medium load conditions, thereby allowing voltage to deviate below or above the rated value. In this paper, V_{dc}^* is kept constant at its rated value, enabling the observation of voltage drop as the load increases.

D. Transition between Droop and Voltage Control Modes in the Battery Converter

Based on the control strategies presented, it can be observed that the battery converter must switch its control mode once the battery is fully charged, transitioning to voltage control mode. Figure 8 shows a complete block diagram of the battery control system.

To prevent undesired and repetitive switching between control modes, a hysteresis block is used to choose the control mode. The converter enters in voltage control mode when $v_{bat} > V_{bat,max}$, and only returns to droop control mode if the battery voltage drops below a smaller value $V_{bat,th}$, called threshold value in this paper. It is important to note that the droop controller $C_d(s)$ is not removed from the system. Instead, when operating in voltage control mode, an additional term is added to the inductor current reference i_L^* . Conversely, when the converter operates in droop control mode, a zero reference is applied to the voltage controller $C_v(s)$, which is also reset.

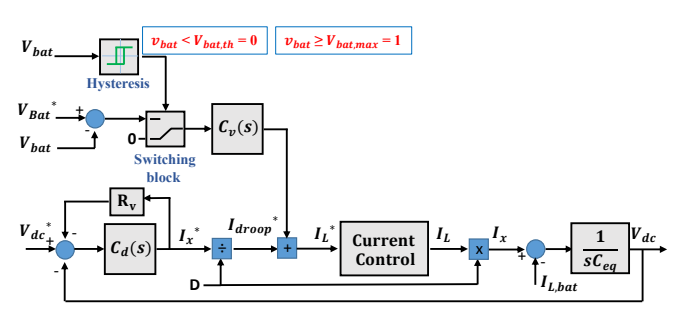


FIGURE 8. Block diagram of the battery controllers, with the transition scheme between droop and voltage control modes.

E. Stability Considerations

Due to the modular structure of the microgrid, a comprehensive analysis of the microgrid stability may be an extensive task using analytical methods. Still, some comments on the stability of the proposed control system are needed. Even with one PV panel and one battery, there is no information shared between these two control systems. With more sources, despite an inefficient current sharing can occur, the microgrid still operates without communication, using the same control principles presented. Therefore, the control system operation and stability should not be affected.

Still thinking in a DC microgrid operating with the proposed control strategy, but with more than a PV panel and a battery, the stability can be compromised by the load conditions. If no load is connected to the DC bus, the batteries can charge. Furthermore, if all batteries are fully charged, the DC bus voltage reaches its maximum value and the PV panels stop injecting current at the DC bus. If the control system is designed correctly, the maximum voltage at the DC bus should be the value V_{dc}^* .

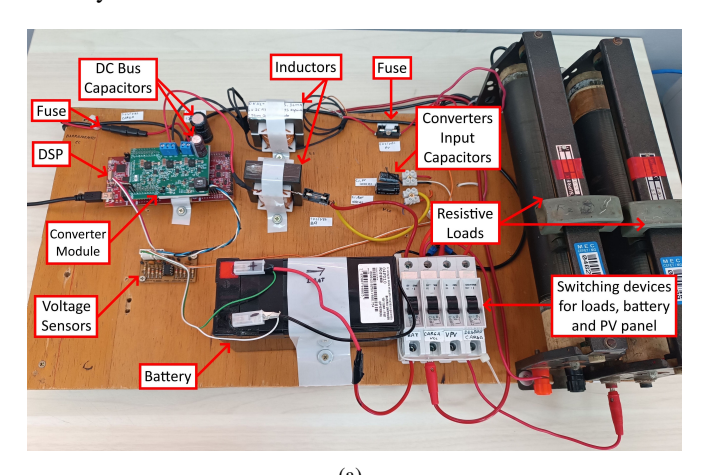
On the other hand, if many loads are connected to the DC bus, the voltage is reduced and more current is injected into the DC bus by the sources. If the load still increases and the DC bus voltage becomes equal to or less than the minimum value, the current supplied by the sources must be limited at a maximum value, in order to preserve the integrity of the microgrid components.

Furthermore, a sharp drop in DC bus voltage can be caused by a fault. In this case, the microgrid control system must be able to identify the fault and interrupt the power supply, even if this means cutting off the entire supply. In this article, this extreme situation is not addressed, as failure analysis requires a dedicated study.

The proposed microgrid was tested in four scenarios, in order to test its performance and stability when different disturbances are applied, such as irradiance variation, successive load connections and a full charge condition of the battery. This will be discussed later, in the results section. In light of the control strategies presented, the following section outlines key aspects of the DC microgrid practical implementation.

III. DC MICROGRID PROTOTYPE IMPLEMENTATION

Figures 9(a), 9(b) and 9(b) show the prototype of the proposed DC microgrid, the PV panel installed on the rooftop and the resistive voltage sensor board, respectively. The converters were implemented using a three-phase converter module BOOSTXL-3PHGANINV. Two half-bridge arms, each one with two metal-oxide-semiconductor field effect transistors (MOSFET) composed of gallium-nitride (GaN), were used as boost converters for the battery and the PV panel. This module has a voltage sensor at the dc bus and current sensors at the low-voltage side, where the inductors are connected. Also, the driver circuits are integrated into the module and the control strategies were implemented in a digital signal processor (DSP) LAUNCHXL-F28379D, directly connected to the converter module.



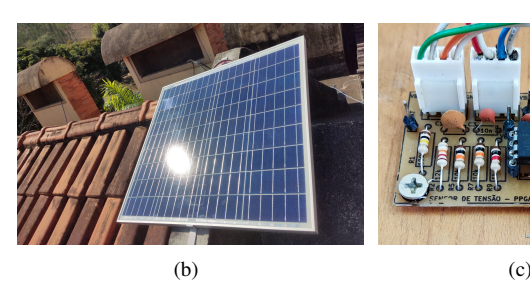


FIGURE 9. Prototype of a DC microgrid: (a) workbench with the converters, battery, sensors, passive filters, DC loads and switching devices; (b) PV panel on the rooftop; (c) resistive voltage sensor board.

Other components used in the implementation of the DC microgrid include a 12 V, 7 Ah Unipower UP1270SEG battery, a 60 W Resun RSM060P PV panel, resistive voltage sensors at the battery and PV panel terminals, capacitor and



inductor filters, protective fuses, resistive loads, and manual switching devices for load connection and disconnection.

Table 1 shows the main parameters of the DC microgrid, including the PV panel, battery, passive filters and DC bus rated values. Based on the proposed control strategy and the presented method to design the controllers, Table 2 shows the controllers gains and the parameters used to design them.

TABLE 1. Main parameters of the DC microgrid, considering the standard test conditions for the PV panel.

Description	Variable	Value	Unit
PV panel rated power	P_{pv}	60	W
PV panel open circuit voltage	$V_{oc,pv}$	22.7	V
PV panel short-circuit current	$I_{sc,pv}$	3.8	A
Capacitance at PV panel terminals	$C_{i,pv}$	1000	μF
Inductance of the PV panel converter	L_{pv}	5.4	mH
Resistance of the PV panel converter	R_{pv}	1.5	Ω
Battery open circuit voltage	$V_{oc,bat}$	13.7	V
Capacitance at battery terminals	$C_{i,bat}$	1000	μF
Inductance of the battery converter	L_{bat}	5.2	mH
Resistance of the battery converter	R_{bat}	1.3	Ω
Battery's maximum charging current	$I_{bat,max}$	1	A
Battery's maximum charging voltage	$V_{bat,max}$	14.5	V
DC bus equivalent capacitance	C_{eq}	1220	μF
DC bus rated voltage	V_{dc}	24	V
DC bus maximum voltage	$V_{dc,max}$	26	V
DC bus minimum voltage	$V_{dc,min}$	22	V
Converter's switching frequency	f_{sw}	20	kHz

TABLE 2. Gains and design parameters of the controller.

Description	Variable	Value	Unit		
PV panel current controller					
Time constant	$ au_{pv}$	1.8	ms		
Proportional gain	$k_{pi,pv}$	3.0	V/A		
Integral gain	$k_{ii,pv}$	861	V/(As)		
Battery current controller					
Time constant	$ au_{bat}$	1.5	ms		
Proportional gain	$k_{pi,bat}$	3.5	V/A		
Integral gain	$k_{ii,bat}$	867	V/(As)		
Battery voltage controller					
Damping ratio	ξ	1.0			
Undamped natural freq.	$\omega_{n,bat}$	168.4	rad/s		
Proportional gain	$k_{pv,bat}$	0.34	A/V		
Integral gain	$k_{iv,bat}$	28.36	A/(Vs)		
Droop controller for both converters					
Damping ratio	ξ	1.0			
Undamped natural freq.	$\omega_{nd,pv}$	266.7	rad/s		
Proportional gain	$k_{pd,pv}$	0.65	A/V		
Integral gain	$k_{id,pv}$	86.76	A/(Vs)		
Virtual impedance	R_v	0.01	Ω		

IV. EXPERIMENTAL RESULTS

In order to test the performance of the proposed control strategy, based on a controlled voltage droop with virtual impedance, it was implemented in the presented DC microgrid. For this, three tests were performed in the DC microgrid:

- 1) Battery charging by CC-CV method;
- 2) Successive load connections;
- 3) Solar irradiance variation.

Following, the results of these three tests will be presented and discussed.

A. Test 1: battery charging by CC-CV method

In this first test, the microgrid operates with a constant DC load of 50 Ω and the sun conditions allow the PV panel to feed the load and charge the battery with maximum current. Figure 10 shows the results of the battery charging process by the CC-CV method, including curves of the DC bus voltage, PV panel voltage and battery voltage and current. Initially, the battery charges with a constant current of 1 A and its voltage increases until it reaches the maximum value 14.5 V. From this moment, with the converter in the voltage control mode, the battery voltage remains constant and its current decreases slowly to complete the charging process. During this process, the DC bus voltage remains almost constant, close to 23 V. Furthermore, the voltage of the photovoltaic panel increases slightly to reduce the power supplied, since the current consumed by the battery decreases.



FIGURE 10. Battery charging by CC-CV method: curves of DC bus voltage, PV panel voltage, battery voltage and current.

Figure 11 shows the same curves of Figure 10 for the charging process with CC-CV method. However, shortly after the control mode switches to constant voltage, the PV panel experiences shading caused by clouds. During the shaded period, the PV panel cannot supply maximum current to the battery. In this case, the battery continues charging, but with a different current than expected, until the clouds disappear. Furthermore, the DC bus voltage is almost unaffected by shading, showing the stability of the control system in such a situation.



FIGURE 11. Battery charging by CC-CV method with a shading event: curves of DC bus voltage, PV panel voltage, battery voltage and current.

B. Test 2: successive load connections

In the second test, the system starts operating without any load connected to the DC bus and the battery charging with constant current. During this test, two loads of 43 Ω and 31 Ω are connected to the DC bus in different moments. Figure 12 shows the DC bus voltage, the PV panel current and the battery voltage and current. The instants t_1 and t_2 indicate the load connections.

Initially, no loads are connected to the microgrid and the battery charges with maximum current of 1 A. After instant t_1 , when the first load is connected, the PV panel current increases and the battery keeps charging, but with a lower current. After instant t_2 , when the second load is connected, the PV panel current does not increase, because it is in the maximum value for the sun conditions. In this last period, the battery begins to supply current to the DC bus, in order to feed the load properly. It is important to note the DC bus voltage, which remains close to 24 V and decreases slightly after t_2 , under heavy load conditions.

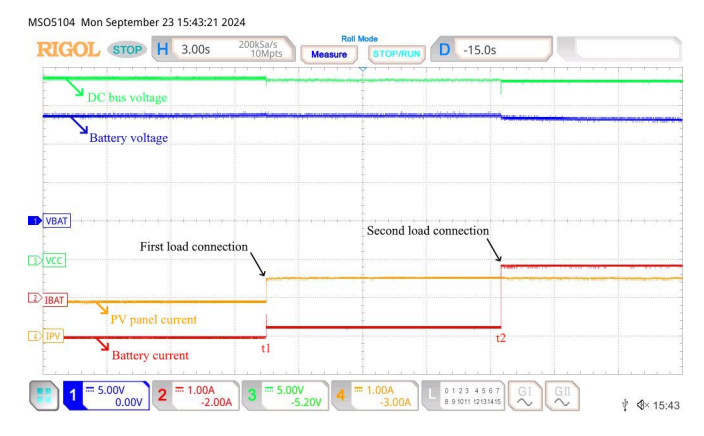


FIGURE 12. Successive load connections at the DC bus: curves of DC bus voltage, PV panel voltage, battery voltage and current.

C. Test 3: solar irradiance variation

In this last test, the DC microgrid operates with constant load of 58 Ω and two artificial shadings are caused on the PV panel. Figure 13 shows the DC bus voltage, the battery current and the PV panel voltage and current. At the beginning, the battery charges with maximum current of 1 A. Between instants t_1 and t_2 , the PV panel is shaded and its voltage and current decrease. During this first interval, the battery current becomes positive and the battery begins to supply power to the DC bus.

After t_2 , the shading stops and the system returns to the previous condition. Between instants t_3 and t_4 , the PV panel is shaded again and this time, the battery supplies a higher current, due to the lower irradiance at the PV panel. It is important to highlight the DC bus voltage behaviour during the entire test, which remains close to 24 V, with small oscillations during the shading periods.

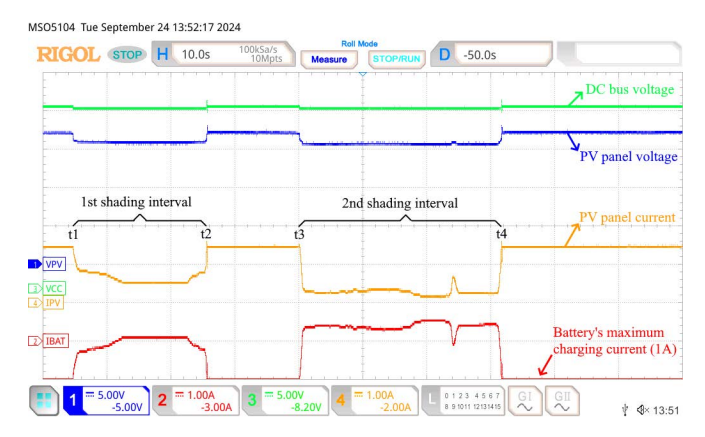


FIGURE 13. Solar irradiance variation: curves of DC bus voltage, PV panel voltage, battery voltage and current.

V. CONCLUSIONS

This paper presented a decentralized control strategy for a DC microgrid, based on a controlled voltage droop with virtual impedance. The proposed approach allowed the management of the energy sources without communication between them and, at the same time, ensuring the DC bus voltage remained between defined bounds. Furthermore, the presented control strategy has shown that a modular expansion of the microgrid, with more sources connected to the DC bus, is possible.

To evaluate the performance of the proposed control strategy, a small-scale prototype of a DC microgrid with a PV panel, a battery and DC loads was implemented. With the experimental tests performed, it was possible to observe the robustness of the control strategy, which was capable of keeping the DC bus voltage between the defined bounds in different operating conditions.

The first test showed the complete charging process of the battery using the CC-CV method. It was possible to observe that the control strategy allows the system to charge the battery while feeding the load, as long as the panel



generates enough power for this. The second test showed how the system behaves in different load scenarios, with the battery charging or supplying power to the DC bus. Finally, in the last test it was possible to observe variations in irradiance, which leads the system to different conditions, with the battery supplementing the energy supplied or using the remaining energy to charge.

It is important to note that the DC bus voltage was kept close to the rated value of 24 V, with small transient oscillations. In the approach used in this paper, the reference value for the droop control was 24 V, therefore, during the operation the DC bus voltage was always below this value. However, it is possible to set this reference above 24 V, allowing the system to operate with rated voltage at full load.

The proposed DC microgrid was implemented using only one PV panel and one battery, However, tests with more PV panels and batteries, as well as other sources, may improve the analysis of the proposed control strategy, since the current sharing can be strongly affected by the droop strategy. In addition, only resistive loads were considered. Despite the instantaneous load connections makes possible to observe the fast response of the microgrid controllers, a further analysis using more complex loads, such as DC motors and linear loads, could be interesting to test the system performance.

A voltage regulation could be added to this control strategy, however, it requires a master converter to regulate the DC bus voltage through its droop reference value. Another option is a management system to set the reference value of the droop control in all converters, which may lead to communication between microgrid components. In this sense, this paper chose to keep the system with zero communication between sources and without a master converter, ensuring the independent operation of the system components.

ACKNOWLEDGEMENT

The authors would like to thank Fundação de Amparo à Pesquisa do Estado de Minas Gerais (FAPEMIG), Conselho Nacional de Desenvolvimento Científico e Tecnológico (CNPq), Coordenação de Aperfeiçoamento de Pessoal de Nível Superior (CAPES) and the Graduate Program in Automation and Systems of CEFET-MG for all support in this research.

AUTHOR'S CONTRIBUTIONS

M.S.LIMA Conceptualization, Data Curation, Formal Analysis, Investigation, Methodology, Software, Validation, Visualization, Writing - Original Draft. R.R.ALMEIDA Conceptualization, Data Curation, Formal Analysis, Investigation, Methodology, Software, Validation. A.O.ALMEIDA Conceptualization, Formal Analysis, Funding Acquisition, Investigation, Methodology, Project Administration, Resources, Supervision, Visualization, Writing – Original Draft, Writing Review & Editing.

PLAGIARISM POLICY

This article was submitted to the similarity system provided by Crossref and powered by iThenticate – Similarity Check.

DATA AVAILABILITY

The data used in this research is available in the body of the document.

REFERENCES

- [1] J. M. Guerrero, R. Kandari, Microgrids: Modeling, Control, and Applications, Academic Press, 2021.
- [2] M. G. Villalva, Energia Solar Fotovoltaica, Editora Érica, 2012.
- [3] R. Zilles, W. N. Macêdo, M. A. B. Galhardo, S. H. F. de Oliveira, Sistemas fotovoltaicos conectados à rede elétrica, Oficina de textos,
- [4] C. Zhao, P. B. Andersen, C. Træholt, S. Hashemi, "Grid-connected battery energy storage system: a review on application and integration", Renewable and Sustainable Energy Reviews, vol. 182, p. 113400, 2023, doi:https://doi.org/10.1016/j.rser.2023.113400.
- [5] F. Kourougianni, A. Arsalis, A. V. Olympios, G. Yiasoumas, C. Konstantinou, P. Papanastasiou, G. E. Georghiou, "A comprehensive review of green hydrogen energy systems", Renewable Energy, p. 120911, 2024, doi:https://doi.org/10.1016/j.renene.2024.120911.
- [6] A. El-Shahat, S. Sumaiya, "DC-microgrid system design, control, and analysis", Electronics, vol. 8, no. 2, p. 124, 2019, doi:https://doi.org/10.3390/electronics8020124.
- [7] F. S. Al-Ismail, "A Critical Review on DC Microgrids Voltage Control and Power Management", IEEE Access, 2024, doi:https://doi.org/10.1109/ACCESS.2024.3369609.
- [8] R. Mayer, M. B. El Kattel, S. V. G. Oliveira, "Bidirectional DC-DC Converter with Coupled Inductor Fordc-Bus Regulation in Microgrid Applications", Eletrônica de Potência, vol. 25, no. 3, pp. 241-248, 2020, doi:https://doi.org/10.18618/REP.2020.3.0007.
- [9] J. C. Pena, J. A. Silva, M. P. Dias, D. P. Damasceno, L. H. Santos, J. A. Pomilio, "Droop-based Control Strategy to operate a DC Nanogrid under the Net Zero Energy Concept", Eletrônica de Potência, vol. 30, pp. e202529-e202529, 2025, doi:https://doi.org/10.18618/REP.e202529.
- [10] T. A. Fagundes, G. H. F. Fuzato, L. J. R. Silva, A. M. dos Santos Alonso, J. C. Vasquez, J. M. Guerrero, R. Q. Machado, "Battery energy storage systems in microgrids: A review of SoC balancing and perspectives", IEEE Open Journal of the Industrial Electronics Society, 2024, doi:https://doi.org/10.1109/OJIES.2024.3455239.
- [11] M. Shaban, M. A. Mosa, A. Ali, K. Abdel-Latif, "Effect of power sharing control techniques of hybrid energy storage system during fault conditions in DC microgrid", Journal of Energy Storage, vol. 72, p. 108249, 2023, doi:https://doi.org/10.1016/j.est.2023.108249.
- W. Miao, Z. Wang, F. Wang, K. H. Lam, P. W. Pong, "Multicharacteristics arc model and autocorrelation-algorithm based arc fault detector for DC microgrid", *IEEE Transactions on Industrial Electronics*, vol. 70, no. 5, pp. 4875–4886, 2022, doi:https://doi.org/10.1109/TIE.2022.3186351
- [13] P. Pan, R. K. Mandal, "Learning approach based DC arc fault location classification in DC microgrids", 208, Power Systems Research, vol. 107874, p. doi:https://doi.org/10.1016/j.epsr.2022.107874.
- [14] M. Uddin, H. Mo, D. Dong, S. Elsawah, J. Zhu, J. M. Guerrero, "Microgrids: A review, outstanding issues and future trends", Energy Strategy Reviews, vol. 49, p. 101127, 2023, doi:https://doi.org/10.1016/j.esr.2023.101127.
- [15] F. S. Al-Ismail, "DC microgrid planning, operation, and control: A comprehensive review", IEEE Access, vol. 9, pp. 36154-36172, 2021, doi:https://doi.org/10.1109/ACCESS.2021.3062840.
- [16] R. A. Ferreira, M. B. Rodrigues, P. G. Barbosa, "Analysis of an adaptive voltage control of dc microgrids using chil real time simulation", in 2017 Brazilian Power Electronics Conference (COBEP), pp. 1-8, IEEE, 2017, doi:https://doi.org/10.1109/COBEP.2017.8257410.
- U. B. Tayab, M. A. B. Roslan, L. J. Hwai, M. Kashif, "A review of droop control techniques for microgrid", Renewable and Sustainable Energy Reviews, vol. 76, pp. 717-727, 2017, doi:https://doi.org/10.1016/j.rser.2017.03.028.



- [18] X. Lu, J. M. Guerrero, K. Sun, J. C. Vasquez, "An improved droop control method for DC microgrids based on low bandwidth communication with DC bus voltage restoration and enhanced current sharing accuracy", IEEE transactions on power electronics, vol. 29, no. 4, pp. 1800-1812, 2013, doi:https://doi.org/10.1109/TPEL.2013.2266419.
- [19] T. V. Vu, D. Perkins, F. Diaz, D. Gonsoulin, C. S. Edrington, T. El-Mezyani, "Robust adaptive droop control for DC microgrids", Electric Power Systems Research, vol. 146, pp. 95-106, 2017, doi:https://doi.org/10.1016/j.epsr.2017.01.021.
- [20] H. Khoramikia, S. M. Dehghan, S. Hasanzadeh, "Droop control method based on fuzzy adaptive virtual resistance for DC microgrids", International Journal of Power Electronics, vol. 14, no. 2, pp. 197-215, 2021, doi:https://doi.org/10.1504/IJPELEC.2021.117065.
- [21] A. L. Guerra, I. Barbi, "The Virtual Resistor Used in Droop Control of DC Microgrids is a Series Loss-Free Resistor (SLFR)", Eletrônica de Potência, vol. 28, no. 3, pp. 248-255, 2023, doi:https://doi.org/10.18618/REP.2023.3.0022.
- [22] A. O. Almeida, P. M. Almeida, P. G. Barbosa, "Design Methodology for the DC Link Current Controller of a Series-Connected Offshore Wind Farm with a Droop Control Strategy", IEEE Transactions on Industry Applications, 2024, doi:https://doi.org/10.1109/TIA.2023.3335028.
- [23] D. H. Santos, B. A. Coutinho, A. S. Cordeiro, M. M. Stopa, A. F. Cupertino, "A Case Study of a Didactic Platform Experiments using Off-the-Shelf Hardware", Eletrônica de Potência, vol. 30, p. e202501, 2025, doi:https://doi.org/10.18618/REP.e202501.
- [24] K. Ogata, Modern Control Engineering, 5 ed., Prentice Hall, 2009.
- [25] R. R. Kumar, C. Bharatiraja, K. Udhayakumar, S. Devakirubakaran, S. Sekar, L. Mihet-Popa, "Advances in batteries, battery modeling, battery management system, battery thermal management, SOC, SOH, and charge/discharge characteristics in EV applications", IEEE Access, 2023, doi:https://doi.org/10.1109/ACCESS.2023.3318121.

BIOGRAPHIES

Maico S. Lima holds a degree in Control and Automation Engineering (2020) and a Master's degree in Automation and Systems (2024) from the Federal Center for Technological Education of Minas Gerais (CEFET-MG). Since 2015, he has worked as a laboratory technician at CEFET-MG, Campus Leopoldina.

Renan R. Almeida is Electrical Technician (2021) and he is currently undergraduate student of Control and Automation Engineering, since 2019, both at Federal Center for Technological Education of Minas Gerais (CEFET-MG), Campus Leopoldina.

Andrei O. Almeida received the B.S., M.Sc., and Ph.D. degrees in Electrical Engineering from the Federal University of Juiz de Fora (UFJF), MG, Brazil, in 2017, 2019 and 2023, respectively. Since 2019, he has been professor at Federal Center for Technological Education of Minas Gerais (CEFET-MG), Campus Leopoldina. Since 2023, he has been professor of the Graduate Program in Automation and Systems (PPGAS).

